Sensors and Actuators B 241 (2017) 99–108

Contents lists available at ScienceDirect

Sensors and Actuators B: Chemical

journal homepage: www.elsevier.com/locate/snb

Conduction mechanisms in SnO_2 single-nanowire gas sensors: An impedance spectroscopy study

F. Schipani[a,b], D.R. Miller[a,c], M.A. Ponce[b], C.M. Aldao[b], S.A. Akbar[a,*], P.A. Morris[a], J.C. Xu[c]

[a] Department of Materials Science and Engineering, The Ohio State University, Columbus, OH 43212, United States
[b] Institute of Materials Science and Technology (INTEMA), University of Mar del Plata and National Research Council (CONICET), B7608FDQ Mar del Plata, Argentina
[c] NASA Glenn Research Center, Cleveland, OH 44135, United States

ARTICLE INFO

Article history:
Received 29 May 2016
Received in revised form 4 October 2016
Accepted 14 October 2016
Available online 14 October 2016

Keywords:
Impedance spectroscopy
SnO_2
Single nanowire
Multiple nanowire
Equivalent circuit

ABSTRACT

Results of studies on single and multiple SnO_2 nanowire gas sensors with impedance spectroscopy are reported. Equivalent circuit modeling is used to draw fundamental conclusions about the dominant conduction mechanism in single-nanowire sensors, where the diameter of the nanowire is found to play a key role. This is then extended to multiple-nanowire sensors. For single-nanowire sensors, I–V measurements are also used to demonstrate that the contribution from the electrode-nanowire contact to the overall resistance changes with atmosphere and temperature. We find that for the randomly-orientated multiple-nanowire sensors, the main contribution to the resistance comes from the nanowire–nanowire junction.

1. Introduction

There is an increasing need for low-cost, low-power and highly sensitive gas sensors for commercial and industrial applications in health and safety areas such as hazardous gas monitoring, medical diagnosis, emission control in combustion processes and many other. Over the last few decades, resistive-type polycrystalline oxides have been used in gas sensors due to simple and low-cost fabrication, but their sensitivity, selectivity and response time need further improvements [1–5]. Nanostructures are meeting these needs with a higher surface-to-volume ratio that increases the interaction between the gas species and the surface. These structures are extensively studied and there are many synthesis routes to obtain those [6,7]. Commercial production of crystalline nanowires is becoming affordable and reproducible at industrial scales [8]. Many researchers design gas sensors based on these nanowires that are highly sensitive and selective to different gases, but the general approach to improve these devices is a trial-and-error method. Impedance spectroscopy is a novel approach to understand these materials and guide design of new nanostructures, as highlighted by a recent review [41]. It gives the same information as the usual DC measurements that the vast majority of researchers use, but also yields fundamental information about the physicochemical processes that govern the electrical response, such as electrode interface contributions, bulk and surface reaction with different gases [9–12].

In this work, single-nanowire and multiple-nanowire SnO_2 gas sensors were tested toward different gases and temperature conditions with the goal of understanding the conduction mechanism that governs the electrical response. Single-nanowire and multiple-nanowire sensors were measured using I–V curves along with impedance spectroscopy measurements to quantify the Pt electrode-nanowire contact and the intrinsic nanowire contribution separately. An equivalent circuit model that reflects these data was then proposed to explain the conduction mechanism as a function of nanowire diameter, operating temperature, and atmospheric oxygen content.

2. Conduction mechanisms

A Schottky barrier is a potential energy barrier that is typically present at metal-semiconductor junctions, induced by dissimilar work functions or electron affinities of two materials in electrical contact. This type of energy barrier can be found at any interface including surfaces in which a semiconductor is involved. A Schottky barrier can be characterized by two parameters: height (in energy) and width (in distance). In an n-type semiconductor, oxidizing atmospheres like oxygen have the tendency to increase the

* Corresponding author at: 2041 N. College Road, Columbus, OH 43210, United States.
E-mail address: akbar.1@osu.edu (S.A. Akbar).

http://dx.doi.org/10.1016/j.snb.2016.10.061
0925-4005/

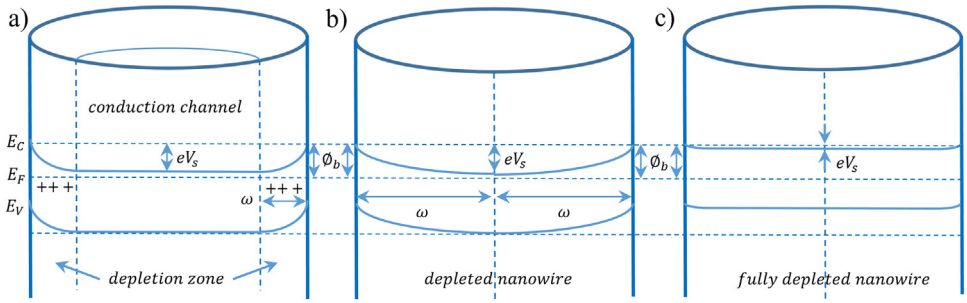

Fig. 1. Band gap diagram in nanowires. (a) A nanowire with a depletion zone at the surface and with free carriers in its center where conductivity is high. This is the depletion width established by surface processes. (b) Due to oxygen in-diffusion, the nanowire center becomes partially depleted. The band bending is the same as in the previous case. The conduction channel width reduces to zero and the conduction through the nanowire decreases significantly. The conduction between the nanowires is also reduced from decreased tunneling. (c) If oxygen in-diffusion continues, it leads to the lifting of the conduction band from E_F and the band bending becomes smaller than ϕ_b. The barrier height remains constant in the whole diffusion process as long as the temperature and atmosphere are kept constant. It is important to point out that when barriers are not overlapped, $\phi_b \approx eV_s$ is regularly considered as a good approximation.

barrier height due to charge accumulation at the interface caused by chemisorbed oxygen bonding with free electrons. This causes a local increase of the electric field which increases the potential, with a maximum at the interface. This barrier can be seen as upward-sloping conduction and valence band edges in Fig. 1. Inert gases such as nitrogen only modify the oxygen coverage of the surface by creating a lower equilibrium oxygen concentration. Barrier width is established by a charge equilibrium between the negatively-charged interface and the compensating positively-charged region depleted of mobile carriers, called the depletion layer.

Electrical properties of oxide semiconductors are usually described by a one-dimensional model representing the interface between two particles. It is also regularly considered that a thermionic (thermally-activated) mechanism is responsible for the sample conductivity and is described by

$$J_{thermionic} = AT^2 e^{-\phi_b/kT}, \tag{1}$$

where $\boldsymbol{\phi_b}$ is the barrier height and is defined as the band bending plus the difference between the conduction band minimum (CBM) and the Fermi level $\phi_b = eV_s + (E_{CBM} - E_F)$ (see Fig. 1). J, T, k and A are current density, the absolute temperature, the Boltzmann constant and the Richardson constant [13], respectively. This equation reflects an activated process due to inter-particle barriers.

Further, it has been pointed out in previous works of the group [14–17] and other researchers [18,19] that an additional tunneling contribution is unavoidable for the usual barrier characteristics and can be calculated as

$$J_{tunneling} = \frac{AT}{k}\int_0^{Vs} F(E) * P(E)\, dE, \tag{2}$$

where $F(E)$ is the Fermi-Dirac distribution function and $P(E)$ is the transmission probability determined by the one-dimensional and time-independent Wentzel-Kramers-Brillouin (WKB) approximation. After integration and for a parabolic barrier, P(E) can be expressed as in Ref. [18]. The total conduction in the sample can be calculated as the sum of both contributions: thermionic and tunneling. *Thus, the thermionic conduction mechanism only depends on barrier height and the tunneling mechanism depends both on barrier height and width.* Eq. (1) indicates that only carriers with energy higher than the barrier contribute to the conduction. Similarly, Eq. (2) accounts for carriers with energies between the CBM and the top of the barrier that contribute to conduction through tunneling. For these kinds of metal oxides, both contributions can be relevant. Tunneling becomes the dominant conduction mechanism as temperature decreases and/or doping increases. [18,19].

When oxygen chemisorbs on the nanowire surface, equilibrium is quickly reached. As stated above, this increases the barrier height [20]

$$\frac{1}{2}O_2(g) + S \leftrightarrow O^0_{ads} \tag{3}$$

$$O^0_{ads} + e^- \leftrightarrow O^-_{ads}, \tag{4}$$

where S corresponds to an adsorption site on the surface and (g) refers to a gas phase. This implies that more ambient oxygen increases chemisorbed oxygen and induces a larger barrier height. Assuming a constant temperature, this process continues until the surface of the material reaches an equilibrium of adsorbed oxygen.

It is considered, as an approximation, that defect states within the band gap above the Fermi level, E_F are empty and below are full. Oxygen chemisorbing on the surface traps conduction electrons at energies that lie within the band gap. This reduction of charge carriers causes the conduction band to bend upwards, away from the Fermi level. Thus, a depletion region of width ω is formed, where electron density is very low [16,21,22].

In SnO_2, oxygen vacancies are the dominant defects and behave as donor impurities with densityN_d. The oxygen exchange equilibrium is regularly written as

$$O^-_{ads} + e^- \leftrightarrow O^{2-}_{int} + S \tag{5}$$

$$V^{2+}_O + O^{2-}_{int} \leftrightarrow O_{latt} \tag{6}$$

There are several steps in these equations: a possible mechanism is that neutral oxygen in the crystal O_{latt} leaves its site to create a doubly ionized vacancy V^{2+}_O and a doubly ionized interstitial O^{2-}_{int}. Then, the oxygen interstitial migrates to the surface and finally becomes neutral to desorb into the gas phase. Eqs. (3)–(6) describe the mechanisms in which oxygen goes from the bulk to the gas phase and vice versa: oxygen adsorption (Eq. (3)), surface ionization (Eq. (4)), bulk incorporation as an ion (Eq. (5)) and finally vacancy annihilation (Eq. (6)).

By adding Eqs. (3)–(6) we obtain

$$V^{+2}_O + 2e^- + \frac{1}{2}O_2 \leftrightarrow O_{latt} \tag{7}$$

and the corresponding mass action law for Eq. (7) is [23]

$$K = \left[V^{2+}_O\right]\left[e^-\right]^2 p(O_2)^{1/2} \tag{8}$$

Square brackets denote concentration and K is the mass action constant or the equilibrium constant. Eq. (8) indicates that, at equilibrium, the oxygen vacancy concentration directly depends on the oxygen partial pressure in the gas phase. Previous studies by this group [14] have shown that the equilibrium barrier height depends

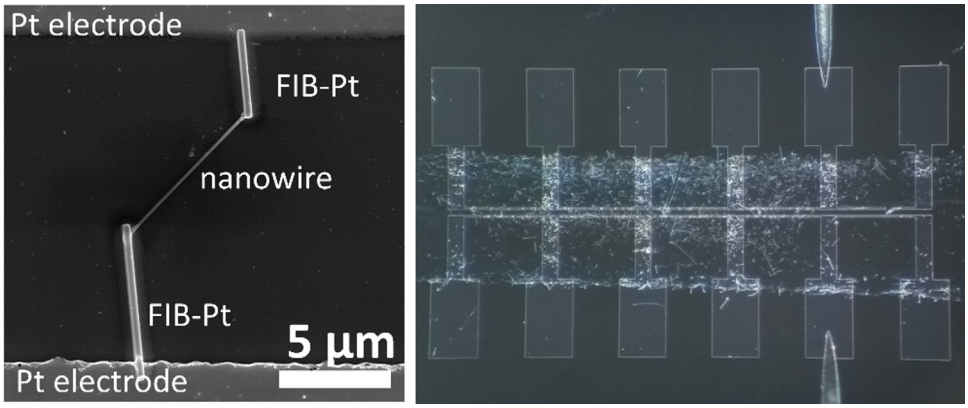

Fig. 2. (a) Example of SEM image of the Pt-SnO_2 contacts made by FIB lithography on a single nanowire; (b) multiple nanowire sensor where a random dispersion of nanowires is shown.

on the surface reactions described by Eqs. (3) and (4). Once established, the barrier height is not significantly affected by subsequent slower changes in the oxygen vacancy concentration dominated by Eqs. (5) and (6).

After a sudden increase in the oxygen pressure, the surface species rapidly evolve through Eqs. (3) and (4) and the barrier height is established. Then, if the temperature is high enough, the oxygen vacancy concentration decreases by means of the slower process of Eqs. (5) and (6). As this takes place, the width of the depletion region expands towards the center of the nanowire. Fig. 1a shows the beginning of this process. Fig. 1b shows the point where the last part of the conduction channel becomes partially depleted and the depletion width, ω, is equal to the nanowire radius. At this point, the conduction band minimum at the center begins to move away from the Fermi level. Further vacancy annihilation leads to total depletion of free electrons in the center of the nanowire, as shown in Fig. 1c. Eventually the CBM has the same value along the entire grain as determined by the surface conditions [24].

It could be expected that the thermionic current increases exponentially as the band bending decreases due to the elevated CBM, but this simultaneously causes the density of electrons to decrease in a similar manner. These two effects mostly compensate if ϕ_b is constant and the thermionic contribution to conductivity is almost not affected if the barrier height does not change [15,25]. The only term strongly affected by the change in donor concentration is the tunneling current because the conduction band electrons see a wider barrier to tunnel through [16,17,26,27]. This process of in/out diffusion in SnO_2 [28], begins at approximately 250 °C and is reversible [14,15]. It is important to note that a small diameter nanowire could be completely depleted by surface processes, depending on the equilibrium chemisorbed oxygen concentration. Using the depletion approximation, the relation between the width of the depletion layer and the donor concentration in a one-dimensional model reduces to Eq. (9) [29]. This equation is the result of considering a one-dimensional model for conduction through the particles and a constant net charge density in the depleted zone.

$$\omega = \sqrt{\frac{2\varepsilon_0\varepsilon_r V_s}{eN_d}} \tag{9}$$

It is also possible that exposure to a reducing or inert gas can cause a fully-depleted thin nanowire to become only partially depleted (see Fig. 1a). In/out diffusion of oxygen becomes more important for fully depleting nanowires that would otherwise still have a conduction channel after surface processes form the initial depletion region.

3. Experimental

The vapor-liquid-solid (VLS) mechanism was used to grow the SnO_2 nanowires. The VLS mechanism uses a catalyst (Au) to form a solid solution with the precursor (Sn) at high temperature. A carrier gas continually supplies the precursor and so the catalyst particle precipitates out the precursor onto the substrate, slowing growth of the nanowire while maintaining a catalyst nanoparticle at the tip. A Leica ACE600 sputter-coater was used to deposit 1.4–10 nm of gold onto (100) p-type Si wafers, depending on the thickness of nanowires desired. A 1 cm^2 gold-coated wafer was then loaded into a quartz tube on an alumina Plate 4 cm downstream of an alumina open-ended half-cylinder containing 0.02 g of SnO powder (99.9% Sigma Aldrich). The tube furnace was ramped to 950 °C in 90 min under a steady flow of 200 sccm 5% H_2/N_2 mixture to prevent oxidation of the SnO precursor. At the growth temperature, the flow was substituted with 350 sccm of 4.8 grade Ar and held for 3 h. After the growth time, all gas flow was shut off and the furnace was cooled as fast as possible. The nanowires were on average 50–200 nm in diameter and 5–50 μm long.

An ultrasonic probe was used to remove the nanowires from the substrate into a dispersion of dimethylformamide (DMF). This solvent was selected because when pipetted onto the substrate and electrodes, the drops tended to dry from the outside in, concentrating the nanowires into a smaller area near the electrode gap. The electrodes were made of 150 nm platinum sputtered onto a silicon *p*-type (100) wafer with a 1 μm SiO_2 layer on top from thermal oxidation. The dispersion was added to the center gap of the electrode in 2 μL drops and incrementally inspected with an optical microscope until the dispersion of nanowires was suitable for use. The electrode gap was 20 μm for the multiple nanowire sensor, and 60 μm for the single nanowire sensor. Gold wires were attached to the contact pads using gold paste and the entire sensor was then annealed at 500 °C for two hours to cure the paste and remove organics from the solvent. The sensors were inserted into a 1" inner diameter quartz tube in a tube furnace with wires extending out of the tube for connection to an Agilent 34972A data acquisition unit for DC measurements or a Solartron 1260 Gain-Phase Impedance Analyzer for AC measurements.

Single-nanowire sensors were fabricated using an FEI Helios NanoLab 600 DualBeam FIB/SEM. The dispersion of nanowires was pipetted in the same way onto the electrodes, inspected with an optical microscope to identify candidate nanowires, and fired at 400 °C for 1 h to remove organics, without attaching gold electrical wires. A Ga^+ ion source of 28 pA current was used to catalyze the Pt metalorganic precursor to form thin Pt strips connecting the nanowires to the existing electrode. The Pt strips were scaled

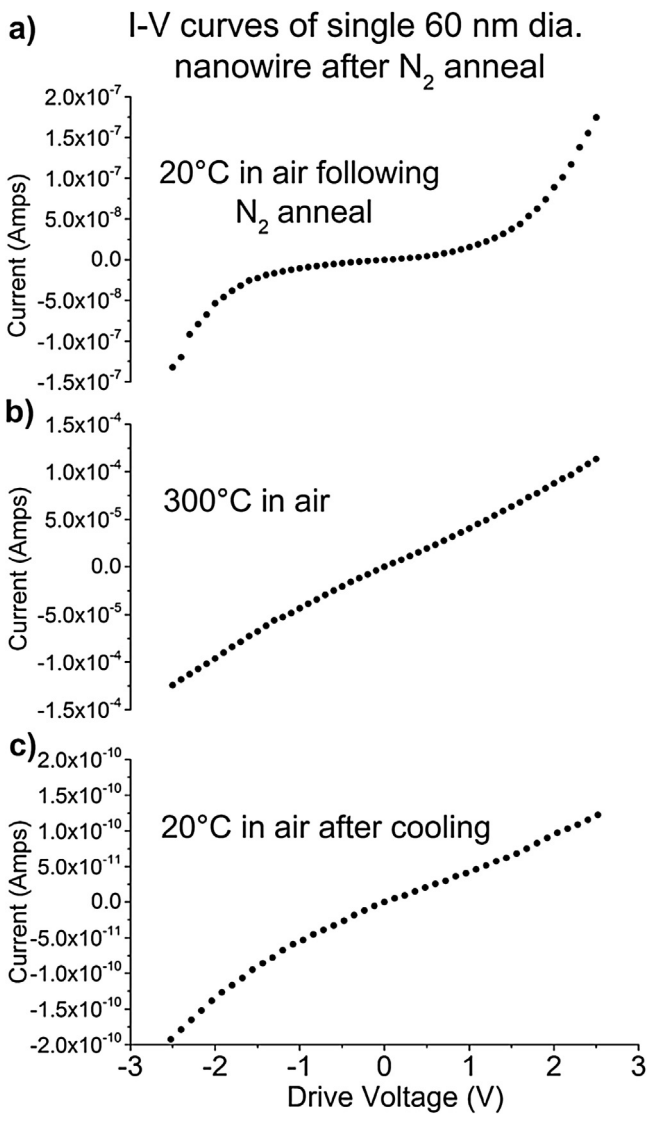

Fig. 3. I–V curves measured at room temperature and at 300 °C for the 60 nm diameter nanowire. (a) The non-linear behavior of the first curve can be associated with a Schottky barrier in the contact zone. (b) After oxygen in-diffusion, the nanowire becomes depleted of mobile carriers (see Fig. 5.IV) and a linear behavior is observed. (c) No diffusion is present in the cooling step and the same linear behavior is observed. Much higher resistance than the first measurement indicates that there is no conduction channel in the center of the nanowire and no Schottky barrier in the Pt-SnO_2 contact which leads to an Ohmic behavior. The linear behavior of the curves shows that the contact no longer dominates the electrical behavior of the sensor.

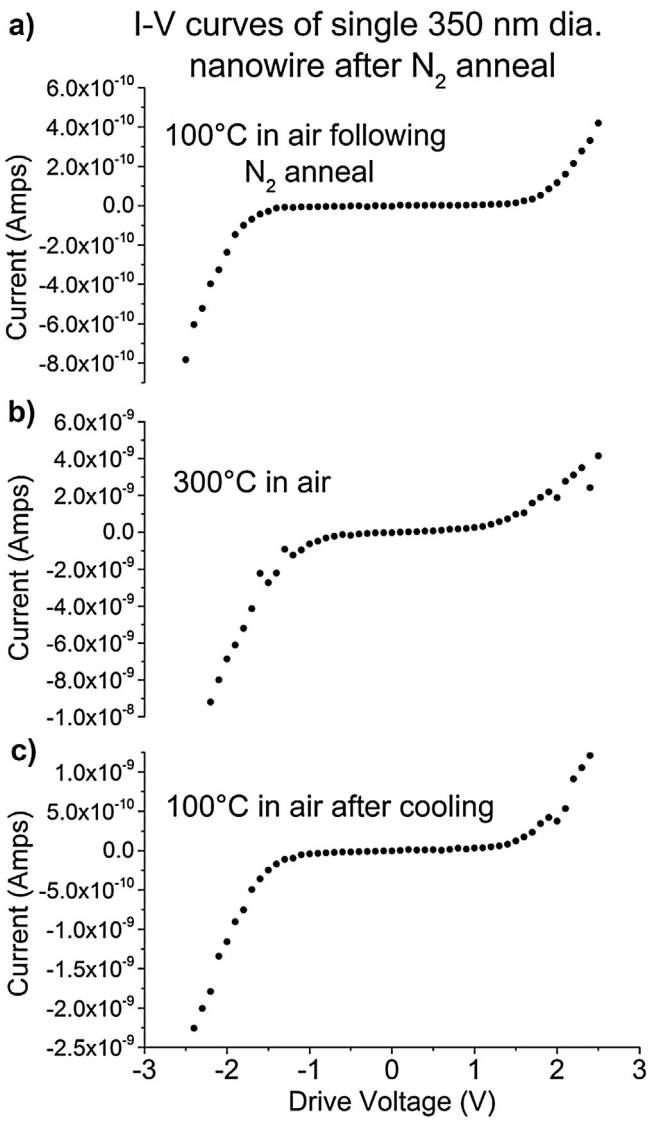

Fig. 4. I–V curves measured at 100 °C and at 300 °C for the 350 nm diameter nanowire analogous to that presented in Fig. 3. Room temperature measurements could not be obtained due to noisy response and high resistance. Here the Schottky-type behavior is present at all temperatures. The changes in the depletion zone width are not enough to fully deplete the nanowire resulting in non-linear response in all cases. The Pt-SnO_2 junction is likely the largest contribution to the total measured resistance.

to approximately the same diameter as each nanowire, typically 200 nm wide and 200 nm thick. Since all six contact pads on each side of the gap were electrically connected in the pre-fabricated electrode, a 980 pA ion beam was then used to mill away the thin sections of the electrodes to electrically isolate a connected single nanowire to the appropriate sets of contact pads. Great care was taken to not expose the nanowire to the ion beam. Only the very ends of each nanowire were exposed to one or two single frame scans at 28 pA, which is not enough to cause morphological changes. After FIB fabrication, gold wires were connected in the same fashion as reported above. The 60 μm gap electrodes were used for single nanowire samples because they gave the most room to find an isolated nanowire and make the Pt FIB connections. The 20 μm gap electrodes were the best for the multiple-nanowire sensors because it maximized the bridging between the pre-deposited electrodes. It was found by SEM inspection that on average more than one nanowire was needed to bridge the 20 μm gap between electrodes, since most nanowires were 10–15 μm long and they were randomly orientated.

Electrical measurements were carried out in the 10^1–10^7 Hz range with an amplitude of 100 mV and no external offset bias was applied unless otherwise stated. The acquired data were represented using a Nyquist plot. Ideally, the contributions of electrode, bulk and interfaces such as grain boundaries and particle–particle contacts can be seen in an impedance plot as separated arcs. Experimentally, arcs can overlap making it difficult to separate them without support from complementary experimental techniques such as I–V curves and the appropriate circuit model. ZPlot® and ZView® software were used to process the impedance data and to build the equivalent electrical circuit models. I–V curves were obtained using a Jmicro Technology LMS-2709 probe station with tungsten tips and heated stage with a Radiant Technologies Precision LC measurement unit, where samples were measured up to 300 °C in air atmosphere.

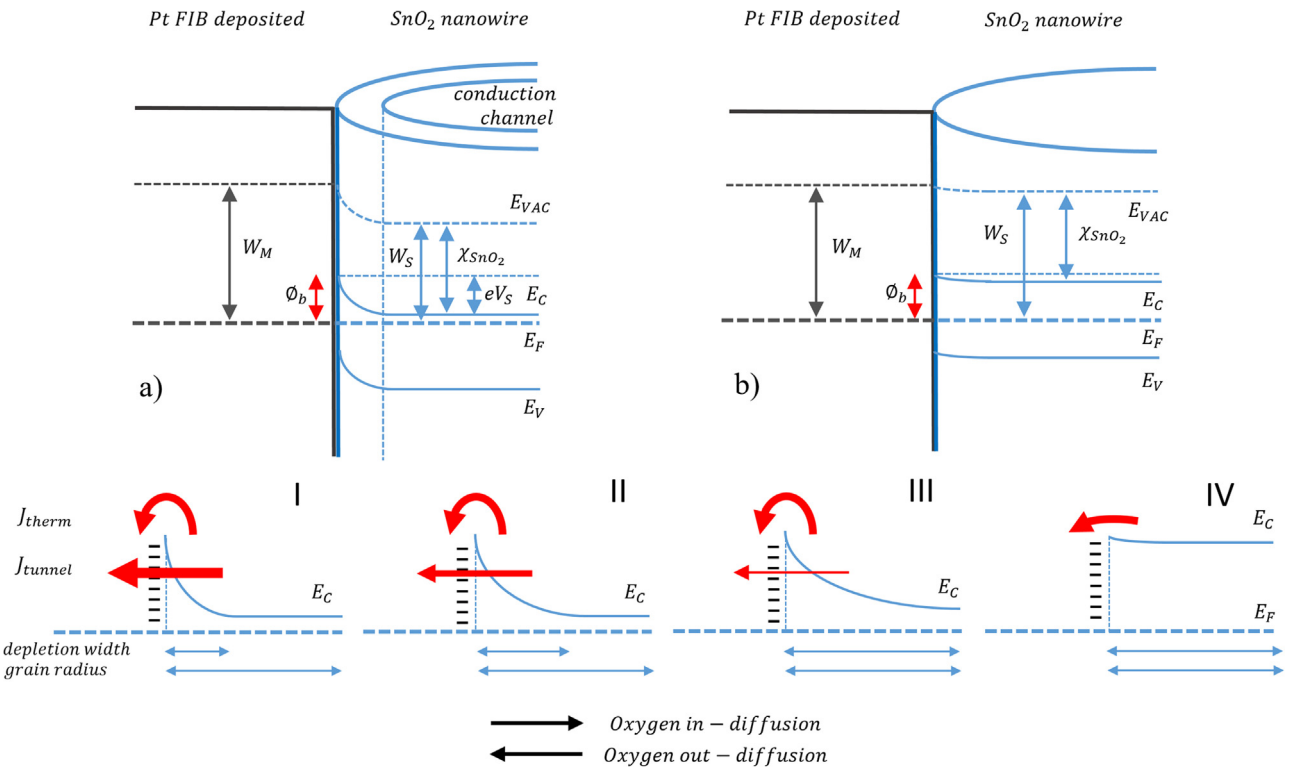

Fig. 5. Schematic view of the Pt-SnO_2 contact that represents the different behaviors measured in the I–V curves shown in Figs. 3 and 4. The first diagram represents the behavior of Fig. 3a and the second diagram represents Fig. 3c where the nanowire is fully depleted of carriers and shows an ohmic behavior due to a flat band condition. Fig. 4 curves are represented by image (a) due to the always-present Schottky barrier. The schematics at the bottom represent the potential barrier at the surface of a nanowire and the effect on the relative current density J as the barrier gets wider (thinner) due to oxygen in- (out-) diffusion. The total current density is the sum of the thermionic and tunneling contributions. When temperature is increased to 300 °C, in-diffusion of oxygen causes the barrier go from I to II. For the thinner nanowire the barrier goes from III to IV. This processes will not be reversible unless a non-oxidizing atmosphere is present at high temperature.

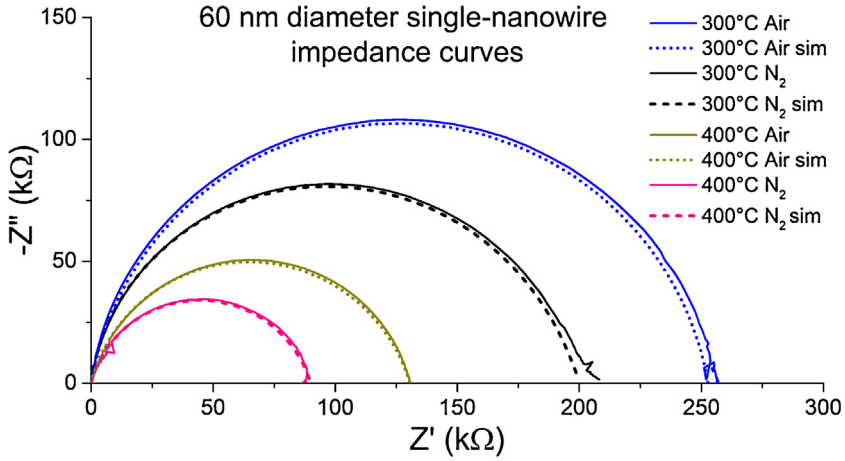

Fig. 6. Impedance plots corresponding to different atmospheres and temperatures for the 60 nm single nanowire sensor. Dashed lines correspond to the fittings made with the equivalent circuit model in Fig. 7.

In Fig. 2, nanowires were imaged using a Nikon Eclipse LV150 optical microscope for the multiple NW sensor, and a FEI Helios NanoLab 600 for the single nanowire sensor with the FIB deposited Pt electrode. Impedance tests were performed inside the quartz tube in 500 sccm flow of 5.0 grade nitrogen and in medical grade breathing air, at several temperatures from 25 °C to 400 °C.

4. Results

4.1. Single-nanowire measurements

Several research groups have used SnO_2 nanowires with FIB-deposited Pt as electrode contacts [30–34]. These studies show that the nature of this contact can have either Ohmic or a Schottky behavior, depending on the atmosphere, temperature [31] and contact area [31,33]. Also, there is some randomness to the quality

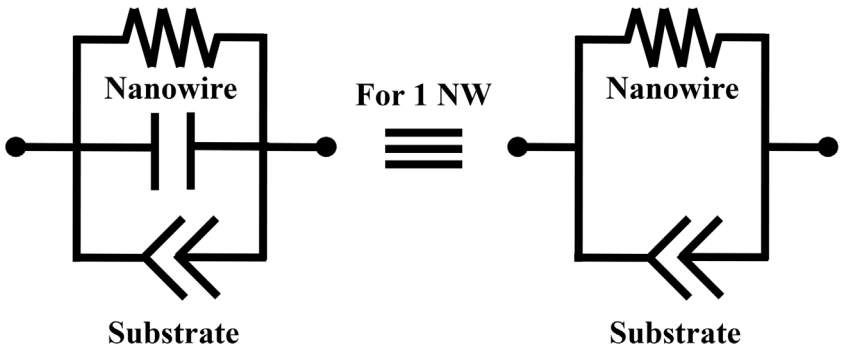

Fig. 7. Equivalent circuit model for a single-nanowire gas sensor. Estimation of the capacitance of a single nanowire is around 0.01 pF, so the circuit was simplified by removing the negligible capacitor element. The substrate is represented by a constant phase elements (CPE) at the bottom. This representation is also valid for high temperatures.

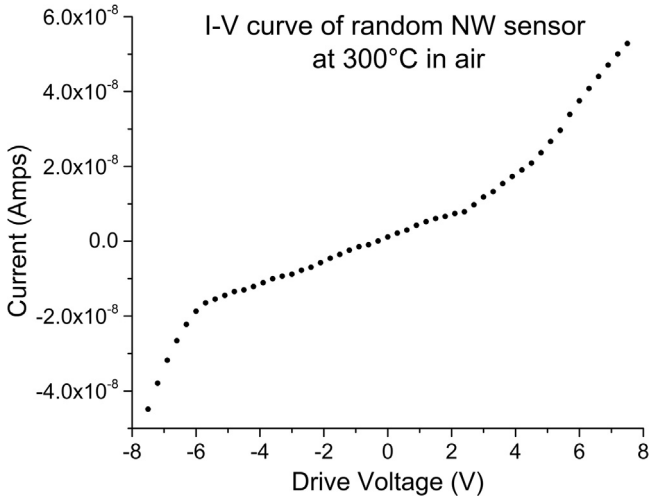

Fig. 8. I–V curve measured at 300 °C in air for the multiple-nanowire sensor. Due to the variation of the nanowire widths, some thin nanowires are completely depleted of carriers but some wider ones are not. Nanowires with a diameter of 100 nm or less (approximately) will not have a Schottky-type contact for our tested conditions; those that are wider may have a conduction channel with free carriers in their center, even for a wide range of temperatures and atmospheres.

of the Pt deposited contacts that can affect the behavior [35]. Here, we analyze this type of device with several techniques. We separate the contributions to the gas sensor response from the bulk of the nanowire and the Pt-SnO_2 contact to build an equivalent circuit model that fully reflects physicochemical changes in the device.

First, current-voltage (I–V) tests were carried out to elucidate the role that the Pt-SnO_2 junction plays on nanowires with different diameters. Fig. 3 and 4 show the measurements of a 60 nm and 350 nm wide nanowire, respectively, performed on a heated stage with a probe station in air at low temperature first, then at 300 °C and finally at low temperature again. Data shown in Fig. 4a and c were measured at 100 °C because the room-temperature resistance was too high to produce a suitable I–V curve. Prior to the first measurement, the samples were exposed to a N_2 atmosphere for 4 h at 400 °C in order to promote temporary reduction in the depletion zone width by removal of adsorbed surface oxygen species and the creation of oxygen vacancies.

Fig. 5 shows a diagram of the junction between the Pt electrode and the nanowire, mimicking the three steps of measurements in Figs. 3 and 4. Fig. 5a is the initial state of the junction, at room temperature and after the nitrogen treatment. Oxygen out-diffusion from the N_2 treatment decreased the depletion region (Eq. (9)) by creating oxygen vacancies and therefore increasing the dopant concentration. This concentration will be "frozen" into the nanowire until heating allows it to reach its air equilibrium concentration. A decreased depletion region leaves an unaffected CBM in the center called the conduction channel. This leaves a large potential barrier for an electron traveling from the bulk to the surface. The metal-semiconductor FIB contact also intrinsically creates a Schottky barrier at the interface of height ϕ_b and a width ω which charge carriers must tunnel through and/or thermionically overcome [19]. As seen in Figs. 3 a and 4, the non-linear behavior is typical of a Schottky junction.

When the sample is measured at 300 °C in an oxidizing atmosphere (Figs. 3 b and 4 b), oxygen diffuses into the nanowire and the depletion zone is enlarged due to annihilation of oxygen vacancies that reduce donor concentration [16,17,26,27]. The linear response in Fig. 3b (60 nm diameter) suggests the nanowire is now fully depleted of carriers which agrees with Ref. [36]. Due to the overlapping of the depletion regions, there is no conduction channel in the center of the nanowire. Electrons now see a potential step and only those with energy higher than this step participate in the conduction. The rest of the electrons can be thought as classical electrons as they cannot tunnel between FIB contacts because the distance is at least 10 μm. This potential is constant and can be thought as a dielectric between two metal electrodes. For this kind of configuration the only possible electrical conduction occurs by means of the Ohmic mechanism. There are not many electrons available for conduction because of the Fermi level position. Those electrons are dragged by the applied field from one contact to the other generating a nearly linear I–V response as seen in Fig. 3b and c. A slight deviation from linearity seen in Fig. 3c is likely a result of some very small remaining Schottky barrier. Thus, the response of the device is controlled mostly by the nanowire itself, with minimal junction resistance. Fig. 4, conversely, shows a different behavior. Here, the wider nanowire (350 nm diameter) is not fully depleted after oxygen in-diffusion. This leaves the CBM at its usual bulk energy in the center of the nanowire resulting in Schottky barriers that cause the non-linear behavior.

Upon cooling in air, the donor concentration remains unaltered from the previous step because the high temperature allowed it to reach its air equilibrium oxygen vacancy concentration. Both Figs. 3 c and 4 c show behavior similar to their previous high-temperature measurement. Fig. 3c does not show the same behavior as Fig. 3a because this 60 nm diameter nanowire is an intermediate thickness that allows it to be fully depleted at high temperature in air but also to have a non-depleted region at its center under high-temperature reducing conditions. In both nanowires, the annihilation of oxygen vacancies at high temperature increased the overall resistance in the later low-temperature measurement. It is important to point out that this marked resistance increase after cooling did not happen when the measurement temperature was kept below 200 °C, which did not allow full oxygen in-diffusion. This is supported by Kamp et al. [23], who estimate the characteristic times of the oxy-

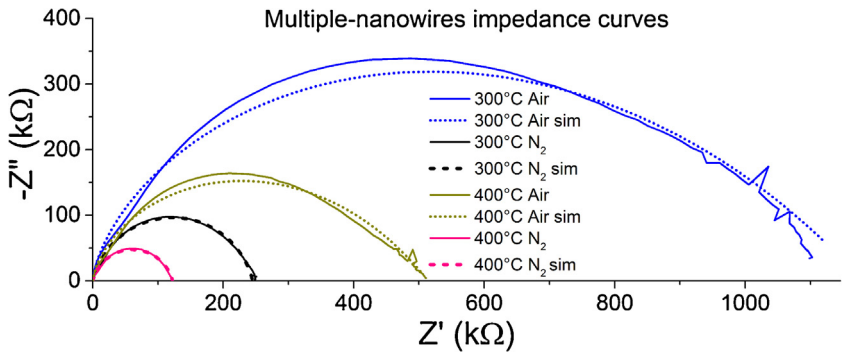

Fig. 9. Impedance plots corresponding to different temperatures and atmospheres in a multiple-nanowire sensor. Dashed lines correspond to the fittings made with the equivalent circuit model in Fig. 9.

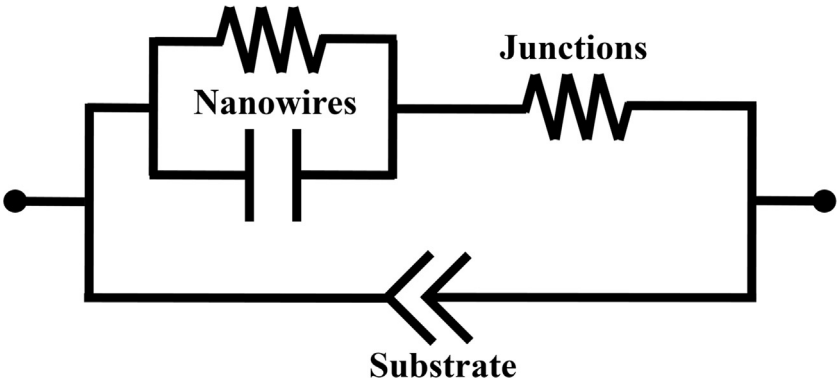

Fig. 10. Equivalent circuit model that includes three different contributions to the overall impedance: junctions between nanowires, nanowires, and the substrate. The main contribution to capacitance comes from the substrate.

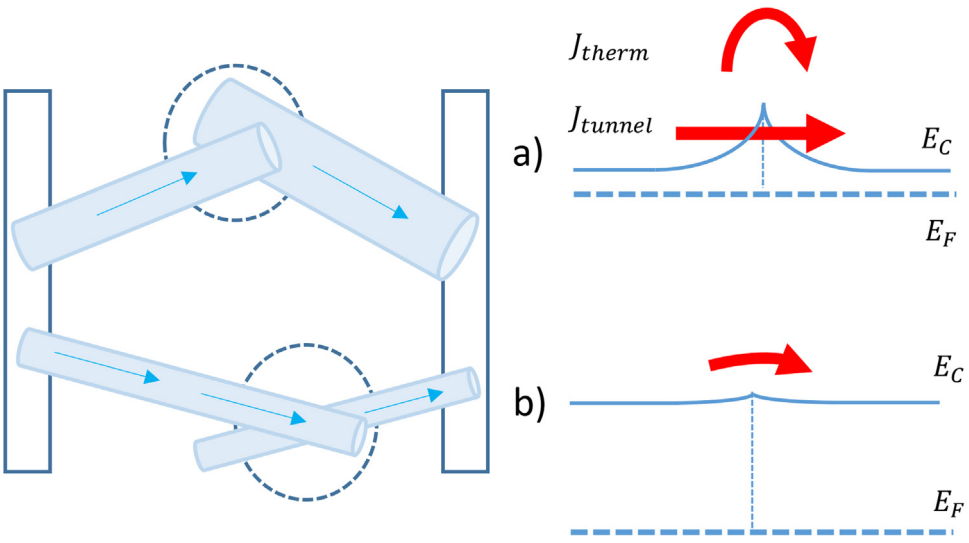

Fig. 11. Schematic view of the multiple-nanowire sensor model. For our model, we consider 500 parallel paths of the two-nanowire contact in series as shown here. In our model, nanowires with the same diameter were considered. In the figure and the real sample, nanowires of several diameters are present. (a) Wide-nanowire junctions show a non-Ohmic behavior as seen in Fig. 4. (b) Thin-nanowire junctions show an Ohmic behavior at high temperature, as seen in Fig. 3.

gen diffusion drift processes depending on temperature and the size of the particle. For an average size of 100 nm, at 300 °C the diffusion from the center of the particle to the surface takes around 10 s and can take several hours at 200 °C, for example. This is an important result because it shows that *the electrical behavior of sensors with Pt-nanowire contacts can depend on the nanowire width*. Lin et al. [31] showed that when Schottky behavior is observed, most of the total measured DC resistance comes from the contact and not from the nanowire.

As metal-semiconductor and bulk contributions compete to dominate the behavior, the addition of randomness in the contact creation seems to complicate the situation. Measurements were done in several sensors and a distinguishable trend was observed, though not systematically predictable. All of the following sensing measurements were carried out at temperatures above 300 °C.

Based on the previous measurements, we can say that when using small nanowires, we expect no appreciable contribution of the Pt-SnO_2 contact, therefore it is not considered in our calculations from here on.

In our goal to separate the varying contributions from the different components of our sensor, we first need to establish some basic calculations. From the depletion approximation, the capacitance per unit area of a Schottky barrier is

$$C = \frac{\varepsilon}{\omega} = \sqrt{\frac{e\varepsilon_r\varepsilon_0 N_d}{2\phi}} \tag{10}$$

and considering typical values for doping concentrations of 1×10^{19} 1/cm^3, relative electric permittivity of 10, and a barrier height of 1 V, we calculate that for a nanowire of 10 μm long and 100 nm wide, the associated capacitance is 8×10^{-15} F. Then, we can approximate that

$$C_{NW} \approx 0.01pF.$$

This is a very small capacitance to be properly measured, especially when other capacitances are there [37]. In further equivalent circuit models, single nanowire capacitance will be neglected and only be considered for comparison purposes with the multiple nanowire equivalent circuit model in the next section.

There is a capacitance between the silicon substrate and deposited Pt electrode. Given the substrate composition, there is a thin SiO_2 layer on the surface that has defects and deep traps which contribute to this capacitance and make the substrate temperature- and atmosphere-dependent. This change is in the ±5% range, but given the small values of the nanowire capacitance it is impossible to distinguish this contribution from the substarate contribution. There is also a small change in capacitance from sample to sample. A constant phase element (CPE) is appropriate to model this contribution where non-ideal elements are present. A CPE is an empirical impedance function of the following form:

$$Z_{CPE} = \frac{1}{A(j\omega)^{\alpha}} \tag{11}$$

The constant A determines the impedance modulus and the exponent α determines the impedance angle which goes from 0° to 90°. In the special cases of α = 1 (90°), the CPE acts as a pure capacitor with the capacitance equals to A and with α = 0 the element behaves as a pure resistance. The main effect of this function in an impedance plot is to distort the semicircle.

Fig. 6 shows impedance measurements performed in the tube furnace with controlled atmosphere under air and 5.0 grade N_2. An AC signal with an amplitude of 100 mV was used and no external (or offset) bias was applied. Dashed lines correspond to fittings made with the circuit of Fig. 7 and show good agreement in the entire frequency range. Similarities in both arcs reveal that a change in the conduction mechanism is unlikely from nitrogen to air measurement.

It can be seen from Fig. 6 that the radius of the semicircle becomes smaller with increasing temperature, indicating a resistance decrease. This is an expected outcome since current transport mechanisms are thermally activated. However, the experimental data cannot be modeled with a simple RC circuit, because the semicircles are not perfect, having a reduced height. The proposed circuit model of Fig. 7 is very simple, but is able to simulate the acquired data properly. This model should not be used at low temperatures where the contribution of the Pt-SnO_2 contact to the total measured resistance has a different contribution which may depend on the last high temperature treatment (see Fig. 3a and c). It should be noted that the semicircles in Fig. 6 are not due to the capacitance contribution of the nanowire, but they reflect the capacitance of the Si/SiO_2 substrate instead, which is modeled with a CPE.

Impedance measurements were also performed on the 350 nm single-nanowire sensor and the results are as expected. The resistance is the same order of magnitude and the impedance arc has the same shape as the 60 nm nanowire. In theory, the large nanowire should show a different contribution to capacitance due to the change in the conduction channel width in the center when exposed to different gases and/or temperature changes. However, as explained above, the magnitude of these changes are too small compared to the substrate capacitance quantified by the model. Yet, the fact that the resistance is in the same order of magnitude and the obtained I–V curves are always non-linear tell us that most, if not all, contributions to resistance come from the Pt-SnO_2 contacts. Additionally, the non-linear I–V curves of both nanowires increase in slope at approximately the same voltage, which shows that the Schottky barrier heights at the interfaces are similar as would be expected when the same two materials are used in both cases.

4.2. Multiple-nanowire measurements

Multiple-nanowire gas sensors were tested under the same conditions as the single-nanowire sensor. They have a 40 μm smaller pre-deposited electrode gap than the single-nanowire sensors which increases the calculated sample substrate capacitance by approximately 30% [38]. Fig. 8 shows an I–V curve for the multiple-nanowire sensor. It was not possible to obtain the same low-temperature I–V curves as the single-nanowire sensor because the resistance was too high and the signal too noisy. The applied voltage is divided between all nanowire–nanowire junctions, so the I–V curve was run up to 7 V instead of 2.5 V due to the number of interfaces present. It is worth noting that the resistance calculated from the I–V curve is higher than that from the impedance arcs at 0 Hz. These discrepancies have been observed on multiple occasions. It is not clear if this is a result of different experimental setups in these measurements or a real effect from the materials.

Impedance measurements in Fig. 9 show that the sensitivity to oxygen in multi-nanowire sensor is larger than the single-nanowire sensor. To separate contributions from the substrate and the nanowires, a simple model was used. Here 1000 nanowires were considered as a rough approximation, however the calculation shows that the conclusion would not change if this number is a few times smaller or larger. The gap between the platinum electrodes is now 20 μm. This allows a few nanowires, which are 10 μm long on average, to span the electrodes when randomly deposited. So, we will consider the distribution of the nanowires in the model as 500 parallel sets of two nanowires in series.

Since the current is divided over the parallel paths each nanowire has 1/250 of a single nanowire contribution. Each nanowire of the pair of bridging nanowires now has half of the capacitance that a single bridging nanowire would have, so all nanowires collectively have an approximate capacitance value of 2.5 pF.

$$C_{1000NWs} \approx 2.5pF$$

Given the amount of parallel paths for the current, the measured resistance now should have been much smaller, but the values are in the range of the single nanowire sensors and even higher. We attribute this to the contact between nanowires, which in our model is represented as 500 parallel resistances, so each junction would have a resistance of approximately 500 MΩ. The contact area between two nanowires can be several times smaller than that of the Pt-nanowire contact because the deposited Pt molds around the nanowire. If we consider that the nanowires are using their whole cross-section to contact each other (highly unlikely) the junction

Table 1
Equivalent circuit data fittings from single-nanowire measurements. The nanowire capacitance value is included but makes no difference in the fittings due to their small value.

SNW at 300 °C	In N_2	In air
Resistance (kΩ)	202	250
NW Capacitance (pF)	0.01	0.01
CPE Amplitude (pF)	650	640
CPE Phase	0.88	0.89

Table 2
Equivalent circuit model data fittings from multiple-nanowire measurements. Here, junction resistance dominates the electrical behavior. CPE amplitude does not represents substrate capacitance in a direct way. Simulated nanowire capacitance has the same order of magnitude as our model.

RNW at 300 °C	In N_2	In air
NWs Resistance (kΩ)	0.1	0.1
NWs Capacitance (pF)	10	10
Junctions Resistance (kΩ)	250	1200
CPE Amplitude (pF)	450	500
CPE Phase	0.85	0.78

between two nanowires would be approximately 8×10^{-15} m^2, and using the same parameters as before, we can estimate the junction capacitance of a single contact as 0.00006 pF. This capacitance cannot be measured.

It is important to point out that the condition of "best fit" for the experimental data is not necessarily the right fit. One needs to develop a circuit model that represents the physical properties of the conduction processes in the sample, as MacDonald states in Ref. [39].

Fig. 10 shows the equivalent circuit used for modeling the multiple-nanowire sensor, where junction resistance is now dominant and the asymmetry in the impedance arcs can be due to the dispersion introduced by the nanowires with different diameters. To model the same response at all frequencies other circuits can be built [40]. One can always find an equivalent circuit to model the experimental data but some models can have an excess of elements, making it very easy to tweak a simulated signal to match the experimental result. It is important to check that the fitted elements make physical sense, as the one built here in Fig. 10.

In this sensor there is a distribution of nanowires diameters that are in contact. If the nanowire is wide enough, it has a region in its center that remains unaltered from surface phenomena (see Figs. 11 a and 5 a). If the nanowires are thinner, then they are depleted of carriers and the contact between them is Ohmic or almost Ohmic (see Figs. 11 b and 5 b) at high temperature. The observed behavior in Fig. 8 is an average response of some Ohmic contacts and some Schottky contacts between the nanowires. Response to oxygen atmosphere in this sample is different from that of the single-nanowire case due to the role played by nanowire–nanowire interfaces, which seems to be more sensitive.

The values in Table 2 can be explained as follows. When a single nanowire was measured (see Table 1), the resistance increased 20% from nitrogen to air atmosphere. This would imply that a single nanowire is not very sensitive to ambient gases. On the other hand, for the multiple-nanowire sensor, the overall resistance increased 480% in the same experimental conditions. The data presented above shows that this is most likely due to the nanowire–nanowire junctions that charge carriers encounter in their conduction path. Our results indicate that these junctions are considerably more sensitive to gas changes.

5. Conclusions

Single-nanowire and multiple randomly-oriented nanowire SnO_2 gas sensors were made. For the single-nanowire sensor, FIB deposited Pt strips were used to contact the nanowire to a pre-deposited electrode. It was determined that above 300 °C for the thin (60 nm dia.) nanowire, the contribution of the contact was not relevant to the total response. This indicates that thin nanowires can be considered as fully depleted and that they are responsible for the resistance changes to the tested gases. For multiple-nanowire gas sensors with a distribution of sizes, it was concluded that the junctions between nanowires had a larger contribution toward the resistance change than the conduction channel width modulation in the nanowires themselves. These junctions have both Ohmic and non-Ohmic responses depending on the diameter of the nanowires forming the junction. The measured response is an average of those two types of contacts. Equivalent circuit models are proposed to fully characterize these behaviors.

Acknowledgment

The current work was partially supported by a Fulbright/BEC.AR Fellowship and by a NASA Space Technology Research Fellowship.

References

[1] G. Korotcenkov, Metal oxides for solid-state gas sensors: what determines our choice? Sci. Mater. Eng. B 139 (2007) 1–23, http://dx.doi.org/10.1016/j.mseb.2007.01.044.
[2] G. Korotcenkov, Gas response control through structural and chemical modification of metal oxide films: state of the art and approaches, Sens. Actuators B Chem. 107 (2005) 209–232, http://dx.doi.org/10.1016/j.snb.2004.10.006.
[3] N. Barsan, M. Schweizer-Berberich, W. Göpel, Fundamental and practical aspects in the design of nanoscaled SnO2 gas sensors: a status report, Fresenius J. Anal. Chem. 365 (1999) 287–304, http://dx.doi.org/10.1007/s002160051490.
[4] J. Tamaki, High sensitivity semiconductor gas sensors, Sens. Lett. 3 (2005) 89–98.
[5] G. Eranna, B.C. Joshi, D.P. Runthala, R.P. Gupta, Oxide materials for development of integrated gas sensors: a comprehensive review, Crit. Rev. Solid State Mater. Sci. 29 (2004) 111–188, http://dx.doi.org/10.1080/10408430490888977.
[6] D.R. Miller, S.A. Akbar, P.A. Morris, Nanoscale metal oxide-based heterojunctions for gas sensing: a review, Sens. Actuators B Chem. 204 (2014) 250–272, http://dx.doi.org/10.1016/j.snb.2014.07.074.
[7] M.M. Arafat, B. Dinan, S.A. Akbar, A.S.M.A. Haseeb, Gas sensors based on one dimensional nanostructured metal-oxides: a review, Sensors (Basel). 12 (2012) 7207–7258, http://dx.doi.org/10.3390/s120607207.
[8] N. Ramgir, N. Datta, M. Kaur, S. Kailasaganapathi, A.K. Debnath, D.K. Aswal, et al., Metal oxide nanowires for chemiresistive gas sensors: issues, challenges and prospects, Colloids Surf. A Physicochem. Eng. Aspects 439 (2013) 101–116, http://dx.doi.org/10.1016/j.colsurfa.2013.02.029.
[9] M.A. Ponce, C.M. Aldao, M.S. Castro, Influence of particle size on the conductance of SnO2 thick films, J. Eur. Ceram. Soc. 23 (2003) 2105–2111, http://dx.doi.org/10.1016/S0955-2219(03)00037-2.
[10] V. Brynzari, G. Korotcenkov, S. Dmitriev, Simulation of thin film gas sensors kinetics, Sens. Actuators B Chem. 61 (1999) 143–153, http://dx.doi.org/10.1016/S0925-4005(99)00285-3.
[11] G. Sakai, N. Matsunaga, K. Shimanoe, N. Yamazoe, Theory of gas-diffusion controlled sensitivity for thin ® lm semiconductor gas sensor, Sens. Actuators B Chem. 80 (2001) 125–131, http://dx.doi.org/10.1016/S0925-4005(01)00890-5.
[12] N. Barsan, U. Weimar, Understanding the fundamental principles of metal oxide based gas sensors, J. Phys. Conden. Matter 15 (2003) 813–839.
[13] C.R. Crowell, Richardson constant and tunneling effective mass for thermionic and thermionic-field emission in schottky barrier diodes, Solid State Electron. 12 (1969) 55–59.
[14] F. Schipani, M.A. Ponce, E. Joanni, F.J. Williams, C.M. Aldao, Study of the oxygen vacancies changes in SnO2 polycrystalline thick films using impedance and photoemission spectroscopies, J. Appl. Phys. 116 (2014) 194502, http://dx.doi.org/10.1063/1.4902150.
[15] C.M. Aldao, F. Schipani, M.A. Ponce, E. Joanni, F.J. Williams, Conductivity in SnO2 polycrystalline thick film gas sensors: tunneling electron transport and oxygen diffusion, Sens. Actuators B: Chem. 193 (2014) 428–433, http://dx.doi.org/10.1016/j.snb.2013.11.114.
[16] C. Malagu; A. Giberti, S. Morandi, C.M. Aldao, Electrical and spectroscopic analysis in nanostructured SnO2: long-term resistance drift is due to

in-diffusion, J. Appl. Phys. 110 (2011) 093711, http://dx.doi.org/10.1063/1.3658870.
[17] C.M. Aldao, D.A. Mirabella, M.A. Ponce, A. Giberti, C. Malagu, Role of intragrain oxygen diffusion in polycrystalline tin oxide conductivity, J. Appl. Phys. 109 (2012) 063723, http://dx.doi.org/10.1063/1.3561375.
[18] C.R. Crowell, V.L. Rideout, Normalized thermionic-field (T-F) emission in metal-semiconductor (Schottky) barriers, Solid State Electron. 12 (1969) 89–105, http://dx.doi.org/10.1016/0038-1101(69)90117-8.
[19] F.A. Padovani, R. Stratton, Field and thermionic-field emission in Schottky barriers, Solid State Electron. 9 (1966) 695–707.
[20] T. Sahm, A. Gurlo, N. Bârsan, U. Weimar, Basics of oxygen and SnO2 interaction; work function change and conductivity measurements, Sens. Actuators B: Chem. 118 (2006) 78–83, http://dx.doi.org/10.1016/j.snb.2006.04.004.
[21] C. Malagù, V. Guidi, M.C. Carotta, G. Martinelli, Unpinning of Fermi level in nanocrystalline semiconductors, Appl. Phys. Lett. 84 (2004) 4158–4160, http://dx.doi.org/10.1063/1.1755419.
[22] R.T. Tung, The physics and chemistry of the Schottky barrier height, Appl. Phys. Rev. 1 (2014) 011304, http://dx.doi.org/10.1063/1.4858400.
[23] B. Kamp, R. Merkle, J. Maier, Chemical diffusion of oxygen in tin dioxide, Sens. Actuators B Chem. 77 (2001) 534–542, http://dx.doi.org/10.1016/S0925-4005(01)00694-3.
[24] C. Malagù, V. Guidi, M. Stefancich, M.C. Carotta, G. Martinelli, Model for Schottky barrier and surface states in nanostructured n-type semiconductors, J. Appl. Phys. 91 (2002) 808–814, http://dx.doi.org/10.1063/1.1425434.
[25] C.-W. Nan, A. Tschöpe, S. Holten, H. Kliem, R. Birringer, Grain size-dependent electrical properties of nanocrystalline ZnO, J. Appl. Phys. 85 (1999) 7735, http://dx.doi.org/10.1063/1.370578.
[26] M.A. Ponce, C. Malagu, M.C. Carotta, G. Martinelli, C.M. Aldao, Gas indiffusion contribution to impedance in tin oxide thick films, J. Appl. Phys. 104 (2008) 054907, http://dx.doi.org/10.1063/1.2975216.
[27] M.A. Ponce, M.S. Castro, C.M. Aldao, Influence of oxygen adsorption and diffusion on the overlapping of intergranular potential barriers in SnO2 thick films, Mater. Sci. Eng. B 111 (2004) 14–19, http://dx.doi.org/10.1016/j.mseb.2004.01.004.
[28] N. Barsan, U. Weimar, Conduction model of metal oxide gas sensors, J. Electroceram. 7 (2001) 143–167, http://dx.doi.org/10.1023/A:1014405811371.
[29] E.H. Rhoederick, R.H. Williams, Metal-Semiconductor Contacts, Clarendon Press, 1988.
[30] J. Huh, J. Na, J.S. Ha, S. Kim, G.T. Kim, Asymmetric contacts on a single SnO2 nanowire device: an investigation using an equivalent circuit model, ACS Appl. Mater. Interfaces 3 (2011) 3097–3102, http://dx.doi.org/10.1021/am2006096.
[31] Y.-F. Lin, C.-H. Chang, T.-C. Hung, W.-B. Jian, K. Tsukagoshi, Y.-H. Wu, et al., Nanocontact disorder in nanoelectronics for modulation of light and gas sensitivities, Sci. Rep. 5 (2015) 13035, http://dx.doi.org/10.1038/srep13035.
[32] Q. Kuang, C. Lao, Z.L. Wang, Z. Xie, L. Zheng, High-sensitivity humidity sensor based on a single SnO2 nanowire, J. Am. Chem. Soc. (2007) 6070–6071.
[33] Y.F. Lin, W.B. Jian, The impact of nanocontact on nanowire based nanoelectronics, Nano Lett. 8 (2008) 3146–3150, http://dx.doi.org/10.1021/nl801347x.
[34] F. Hernández-Ramírez, A. Tarancón, O. Casals, J. Arbiol, A. Romano-Rodríguez, J.R. Morante, High response and stability in CO and humidity measures using a single SnO2 nanowire, Sens. Actuators B Chem. 121 (2007) 3–17, http://dx.doi.org/10.1016/j.snb.2006.09.015.
[35] M. Chakravorty, K. Das, A.K. Raychaudhuri, J.P. Naik, P.D. Prewett, Temperature dependent resistivity of platinum-carbon composite nanowires grown by focused ion beam on SiO2/Si substrate, Microelectron. Eng. 88 (2011) 3360–3364, http://dx.doi.org/10.1016/j.mee.2011.07.012.
[36] A. Kolmakov, Y. Zhang, G. Cheng, M. Moskovits, Detection of CO and O2 using tin oxide nanowire sensors, Adv. Mater. 15 (2003) 997–1000, http://dx.doi.org/10.1002/adma.200304889.
[37] F. Hernández-Ramírez, A. Tarancón, O. Casals, J. Rodríguez, A. Romano-Rodríguez, J.R. Morante, et al., Fabrication and electrical characterization of circuits based on individual tin oxide nanowires, Nanotechnology 17 (2006) 5577–5583, http://dx.doi.org/10.1088/0957-4484/17/22/009.
[38] D. Pascal, P. Dansas, C. Bru, S. Laval, Accurate analytical determination of the resistance of a semiconducting layer between two coplanar electrodes, Semicond. Sci. Technol. 4 (1989) 633–638.
[39] J. Macdonald, W.B. Johnson, Impedance Spectroscopy: Theory, Experiment, and Applications (2nd Edition), 2nd edition, Wiley, 2005.
[40] M.A. Ponce, M.S. Castro, C.M. Aldao, Capacitance and resistance measurements of SnO2 thick-films, J. Mater. Sci. Mater. Electron. 20 (2008) 25–32, http://dx.doi.org/10.1007/s10854-008-9590-8.
[41] F. Schipani, D.R. Miller, M.A. Ponce, C.M. Aldao, S.A. Akbar, P.A. Morris, Electrical characterization of semiconductor oxide-based gas sensors using impedance spectroscopy: A review, Rev. Adv. Sci. Eng. 5 (1) (2016) 86–105.

Biographies

Federico Schipani obtained his B.Sc. in Physics in 2012 in the University of Mar del Plata. He is a Ph. D student in the same university. At the moment he is at the Ohio State University for a research stay. His main interests cover the gas sensing properties and conduction mechanism in grain-based and nanowire-based sensors.

Derek R. Miller is a Ph.D. candidate at The Ohio State University. He began his graduate career in 2011 on an NSF GRFP Fellowship and in 2013 was awarded a NASA NSTRF Fellowship. His research focuses on growing and synthesizing new oxide nanostructures for applications in gas sensing, photovoltaics, and biocompatible surfaces. His recent focus is on fabrication and characterization of oxide nanoheterostructures to enhance performance in these applications. Derek was also the 2013 Chair of the ACerS' PCSA, a national ceramics-focused student organization.

Miguel A. Ponce obtained his B.Sc. in Chemistry in 1999 and PhD in Material Science in 2005 from Mar del Plata National University, Argentina. Since April 2007 he is a member of the research staff of the National Research Council (CONICET). His current research interest includes the development of electronic conduction mechanism of functional inorganic materials.

Celso M. Aldao completed his Ph.D. at the Department of Chemical Engineering and Materials Science of the University of Minnesota in 1989. He was appointed as Professor in 1990 at the University of Mar del Plata. Since 1992 he is a member of the research staff of the National Research Council (CONICET). His research activities focus on the physics and chemistry of surfaces and interfaces, with special emphasis on semiconductors.

Sheikh A. Akbar is a Professor in Materials Science and Engineering at The Ohio State University. He received his Ph.D. in 1985 from Purdue University. He teaches courses on Sensor Materials, Electronic Ceramics, and Thermodynamics. He is the founding director of the NSF Center for Industrial Sensors and Measurements (CISM) and his main research interests include thin film sensors, metal oxide sensors, and nano-textured biomedical coatings.

Pat A. Morris is an Associate Professor in Materials Science and Engineering at The Ohio State University. She received her B.S. from The Ohio State University in 1980 and Ph.D. in 1986 from MIT. Dr. Morris was a Technical Leader working on chemical sensors at Dupont from 1999 to 2005. Her current research interests focus on oxide nanoparticles deposited on miniaturized sensors using ink-jet printing.

Jennifer C. Xu received her Ph.D. in environmental chemistry from the University of Illinois at Urbana-Champaign in 1998. She held a post-doctoral position at Case Western Research University and had mainly worked for Sensor Development Corp, before starting at NASA Glenn Research Center in 2002. Currently she is working on developing chemical microsensors for aerospace applications.